



HAL
open science

Visualization of lipids and proteins at high spatial and temporal resolution via interferometric scattering (iSCAT) microscopy

Susann Spindler, Jens Ehrig, Katharina König, Tristan Nowak, Marek Piliarik, Hannah E. Stein, Richard W. Taylor, Elisabeth Garanger, Sébastien Lecommandoux, Isabel D. Alves, et al.

► To cite this version:

Susann Spindler, Jens Ehrig, Katharina König, Tristan Nowak, Marek Piliarik, et al.. Visualization of lipids and proteins at high spatial and temporal resolution via interferometric scattering (iSCAT) microscopy. *Journal of Physics D: Applied Physics*, 2016, 49 (27), pp.274002. 10.1088/0022-3727/49/27/274002 . hal-01372499

HAL Id: hal-01372499

<https://hal.science/hal-01372499v1>

Submitted on 9 May 2020

HAL is a multi-disciplinary open access archive for the deposit and dissemination of scientific research documents, whether they are published or not. The documents may come from teaching and research institutions in France or abroad, or from public or private research centers.

L'archive ouverte pluridisciplinaire **HAL**, est destinée au dépôt et à la diffusion de documents scientifiques de niveau recherche, publiés ou non, émanant des établissements d'enseignement et de recherche français ou étrangers, des laboratoires publics ou privés.

Visualization of lipids and proteins at high spatial and temporal resolution via interferometric scattering (iSCAT) microscopy

Susann Spindler^{1,2}, Jens Ehrig^{1,3}, Katharina König^{1,2}, Tristan Nowak⁴, Marek Piliarik^{1,5}, Hannah E Stein², Richard W Taylor¹, Elisabeth Garanger⁶, Sébastien Lecommandoux⁶, Isabel D Alves⁷ and Vahid Sandoghdar^{1,2}

¹ Max Planck Institute for the Science of Light, Erlangen, Germany

² Friedrich Alexander University (FAU) Erlangen-Nuremberg, Erlangen, Germany

³ Current address: B CUBE—Center for Molecular Bioengineering, Technische Universität Dresden (TUD), Dresden, Germany

⁴ Optical Imaging Center Erlangen (OICE), Erlangen, Germany

⁵ Current address: Institute of Photonics and Electronics, Academy of Sciences of the Czech Republic, Chaberská 57, Prague, Czech Republic

⁶ Laboratoire de Chimie des Polymères Organiques (UMR5629 LCPO), CNRS, Université de Bordeaux, Pessac, France

⁷ Institute of Chemistry & Biology of Membranes & Nanoobjects (UMR5248 CBMN), University of Bordeaux, Pessac, France

E-mail: vahid.sandoghdar@mpl.mpg.de

Received 20 January 2016, revised 11 March 2016

Accepted for publication 29 March 2016

Published 7 June 2016



Abstract

Microscopy based on the interferometric detection of light scattered from nanoparticles (iSCAT) was introduced in our laboratory more than a decade ago. In this work, we present various capabilities of iSCAT for biological studies by discussing a selection of our recent results. In particular, we show tracking of lipid molecules in supported lipid bilayers (SLBs), tracking of gold nanoparticles with diameters as small as 5 nm and at frame rates close to 1 MHz, 3D tracking of Tat peptide-coated nanoparticles on giant unilamellar vesicles (GUVs), imaging the formation of lipid bilayers, sensing single unlabelled proteins and tracking their motion under electric fields, as well as challenges of studying live cell membranes. These studies set the ground for future quantitative research on dynamic biophysical processes at the nanometer scale.


Keywords: Interferometric detection, light scattering, single-particle tracking, single molecule detection, lipid diffusion, protein detection, single protein electrophoresis

 Online supplementary data available from stacks.iop.org/JPhysD/49/274002/mmedia

(Some figures may appear in colour only in the online journal)

1. Introduction

A fundamental understanding of structure and dynamics in biological systems requires measurement methods that offer

 Original content from this work may be used under the terms of the [Creative Commons Attribution 3.0 licence](https://creativecommons.org/licenses/by/3.0/). Any further distribution of this work must maintain attribution to the author(s) and the title of the work, journal citation and DOI.

the appropriate contrast mechanism as well as sufficient temporal and spatial resolution. In particular, it is highly desirable to visualize various processes down to the level of single biomolecules. Here, optical studies are particularly attractive because they are compatible with live-cell imaging and can be fast and noninvasive. Although the arsenal of light microscopy consists of a number of different contrast mechanisms such as bright field, dark field, and phase contrast, optical approaches

to single molecule biophysics have previously been exclusively based on fluorescence detection.

Unfortunately, single molecule fluorescence microscopy is restrictive in several ways. First, fluorescent emitters photobleach, limiting the total number of emitted photons and, thus, the overall observation time. Second, fluorescence emission saturates. As a result, there is a fundamental limit on the detection speed because at some point, there is no photon in the integration time window. In other words, fluorescence detection puts a severe limit on both the long and short observation times. In practice, this amounts to about 1 ms on the short end and a few minutes on the long time scale. Life science processes, however, span from picoseconds for chemical reactions to days and months for cellular processes, infection and disease development. A third limitation of any label is that it might alter the properties of the biomolecule of interest and its environment, thus causing measurement artefacts. For a concise account of the state-of-the-art fluorescence-based single-particle tracking, we refer the interested reader to [12].

A key technique for single molecule biophysics is spatial localization of a nano-object beyond the diffraction limit. Here, the precision of localizing the particle is dependent on the achievable signal-to-noise ratio (SNR) and therefore the number of detected photons [1, 2]. This in turn demands a certain length of integration time. Fluorescence studies of dynamic processes like diffusion of plasma membrane molecules typically reach a spatial localization precision of 20 to 30 nm within a temporal resolution of about 1 ms [3, 4].

An alternative way to image small molecules is to use elastic scattering instead of fluorescence. Here, one can use a scattering label such as a gold nanoparticle (GNP) or detect the bioparticle directly. In this way, nearly all shortcomings of fluorescence detection are addressed. The linear behaviour of scattering allows one to increase the signal rate by increasing the illumination intensity. Furthermore, lack of photobleaching makes it possible to study the very same single particle for an unlimited period of time. The major trade-off in using elastic scattering as a contrast mechanism is lack of specificity. Indeed, iSCAT turns out to be so sensitive that the signal from nearly every small molecule can be picked up, making it difficult to decipher a specific molecule over the background. Nevertheless, as we discuss below, the method can offer breakthroughs in many situations.

Because the scattered power scales with the square of the particle polarizability α , the scattering signal of very small particles rapidly diminishes as the sixth power of the particle diameter [5]. As a consequence, methods such as dark-field microscopy usually work with gold particles that are 40 nm or larger in diameter [6, 7]. However, as in the case of fluorescence imaging, it is desirable to minimize the size of the marker to avoid geometric hindrance, multiple binding, or drag forces. To ameliorate the fast loss of the scattering signal from small particles, in 2004 we pointed out that one could detect the beat signal between the elastically scattered light and a reference field, which is typically generated by the reflection of the incident beam at the substrate interface [5, 8]. The resulting signal becomes proportional to the scattered field amplitude, thus dropping only as the third power of the

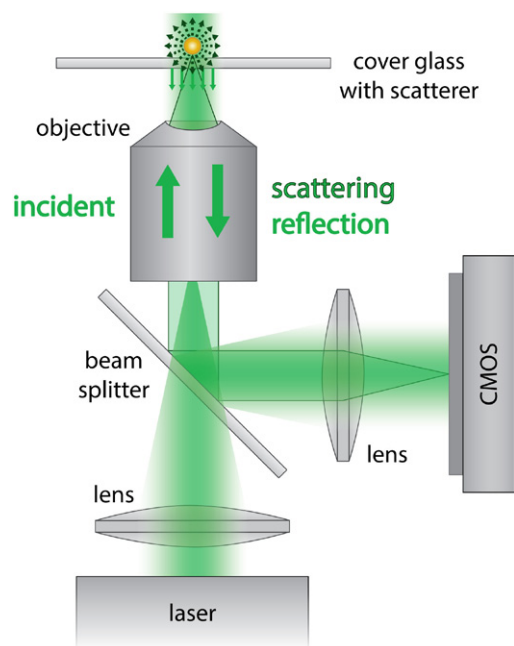


Figure 1. Schematic illustration of the iSCAT setup. A continuous-wave laser is focused onto the back focal plane of a high-NA objective for wide-field illumination. The light reflected by the glass/sample interface and the scattered light from the particle are reflected by a beam splitter onto a CMOS camera.

particle diameter. We coined this interferometric detection of scattered light as ‘iSCAT’ [9].

The contrast in iSCAT is defined as $(I_{\text{det}} - I_{\text{ref}})/I_{\text{ref}}$, where I_{det} and I_{ref} denote the detected signal and the background (reference) intensity, respectively. Although the strength of the reference beam determines the contrast, the sensitivity of the method and the attainable shot-noise-limited SNR depends fundamentally on α [5]. The latter is proportional to the quantity $(\epsilon_p - \epsilon_m)/(\epsilon_p + 2\epsilon_m)$ with ϵ_p and ϵ_m denoting the dielectric functions of the particle and its surrounding medium, respectively. A more important feature of α is, however, its dependence on the particle volume, which in practice dictates the order of magnitude of the iSCAT sensitivity. It turns out that this method allows one to detect even a single small unlabelled protein [10].

2. Experimental setup

A detailed description of the iSCAT setup can be found in [1]. A schematic illustration of the main components is shown in figure 1. Briefly, a linearly polarized continuous-wave laser at 532 nm (or otherwise stated) was used for illumination. The beam passed a beam splitter and was focused onto the back focal plane of an oil-immersion objective, creating a wide-field illumination on the sample of about 3.5 to 10 μm in diameter, depending on the magnification used. The illumination intensity at the objective was 0.01 mW μm^{-2} (or otherwise stated). In some cases, we also used acousto-optic deflectors to scan the laser beam by a few mrad in both lateral directions to increase the area of homogeneous illumination. The scattered and reflected components were collected by the objective, reflected by the beam splitter and imaged onto a CMOS

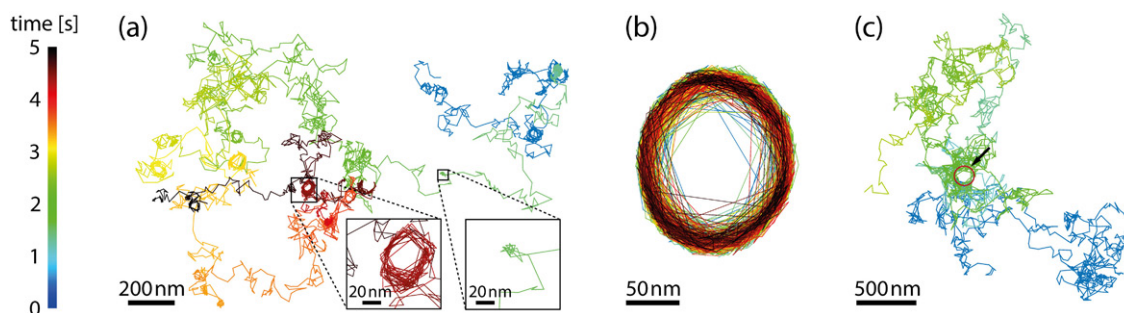


Figure 2. Diffusion of single lipids labelled with 20 nm gold particles within a supported lipid bilayer recorded at 1 kHz for 5 s. The particle position is localized with a precision of about 2 nm. The colour code shows the temporal evolution for all three trajectories. (a) Particle trajectory showing free diffusion, nanoscopic confinement and orbital confinement (DOPC + 0.01 mol-% GM1). (b) Example trajectory of orbital confinement over the whole measurement time (DOPC + 0.025 mol-% GM1). (c) Example trajectory showing Brownian diffusion and an excluded area of around 150 nm in the middle of the trajectory, marked with an arrow and a red circle (DOPC + 0.01 mol-% GM1).

camera (MV-D1024W-CL, Photonfocus AG) or a high-speed CMOS camera (Phantom v1610, Vision Research). Depending on the application, the setup was adapted regarding excitation wavelength and polarization handling. A blueprint description of the hardware and software for iSCAT microscopy will be published elsewhere [13].

3. Measurements using a scattering label

3.1. Tracking 2D lipid diffusion on a supported lipid bilayer

We recently demonstrated tracking of GM1 lipids within supported lipid bilayers (SLBs) of DOPC on glass at a spatiotemporal resolution superior to that achieved with fluorescence [1]. The GM1 lipid molecules were labelled with 20 nm diameter gold nanoparticles via a CTxB linker, and iSCAT videos were recorded at 1 kHz frame rate. Here, it should be mentioned that inertia effects of a particle as small as 20 nm or smaller will not have a considerable influence on the diffusion behaviour of the bound lipid since the viscosity of the buffer solution is around 100 times lower than that of the lipid membrane [13]. In addition to the observation of normal diffusion, the combination of a high localization precision better than 2 nm and a temporal resolution of 1 ms made it possible to observe transient confinement of individual lipid molecules within regions as small as 10 nm, a feature that had previously been undetected in related fluorescence work.

As shown in figure 2(a), we also find intriguing phenomena such as orbital confinement of the diffusing GNP to a ‘race track’. The inset in this figure clearly resolves the width of such tracks to be also of the order of 10 nm. Figure 2(b) displays an example, where the particle remained on the same circular track for at least 5 s. We note that these observations cannot be due to instrumental artefacts since we observed such race-track trajectories at the same time as normal diffusion for other particles (see, e.g. figure S1 of the supplementary data) (stacks.iop.org/JPhysD/49/274002/mmedia). The long duration of our trajectories also reveals nanoscopic and microscopic regions of void, which possibly hint to small defects in the supported bilayer (see figures 2(c) and 3(b)). A clear and quantitative understanding of these observations requires further investigations. We had not included these results in our earlier publication, but similar findings have also

been reported in [14]. It is worth emphasizing that such rare nanoscopic events are impossible to detect with other methods such as fluorescence recovery after photobleaching (FRAP) or slow and less precise tracking experiments.

In [1], we used gold nanoparticles with a diameter of 20 nm. However, as mentioned earlier, iSCAT can even detect smaller particles. In the lower inset of figure 3(a) we show a background-corrected iSCAT image of a 5 nm GNP bound via streptavidin to headgroup-biotinylated DOPE in a DOPC SLB. Figure 3(a) displays a diffusion trajectory of this particle recorded at a frame rate of 23 kHz, which is the maximum speed of the camera (PhotonFocus) for a convenient field of view of 64×64 pixels (corresponding to $4 \mu\text{m} \times 4 \mu\text{m}$ in our configuration). Such a small label is clearly preferable over larger particles because its geometric extent perturbs the lipid membrane much less and because it is unlikely that it carries more than one anchor molecule.

The frame rate mentioned above is limited by the speed of conventional CMOS cameras. However, a nanoparticle can be tracked much faster by using high-speed cameras. Indeed in [15], tracking with speeds up to 100 kHz was demonstrated. Figure 3(b) displays a trajectory for a GNP with a diameter of 20 nm localized at a spatial precision of 9.7 nm recorded at a speed of 913 kHz, the highest speed reported to date for single particle tracking. The difference between the trajectories of figures 3(a) and (b) is striking. Although the overall length of the latter is almost three times shorter, it is considerably fuller. This emphasizes the added value of the high speed for revealing residence events that would otherwise be missed. The high density of the trajectory in figure 3(b) hints to voids and membrane imperfections even more convincingly than in figure 2. In future studies, measurements such as those in figure 3(b) can be performed for much longer times of tens of minutes, spanning a dynamic range of nine orders of magnitude to provide an unprecedented insight into the physics of lipid membranes.

3.2. Tracking 3D diffusion of protein-coated particles on giant unilamellar vesicles

The findings of figures 2 and 3 provide a few examples where artifacts due to the interaction between the lipid molecules and the substrate cannot be ruled out. To get around the difficulties

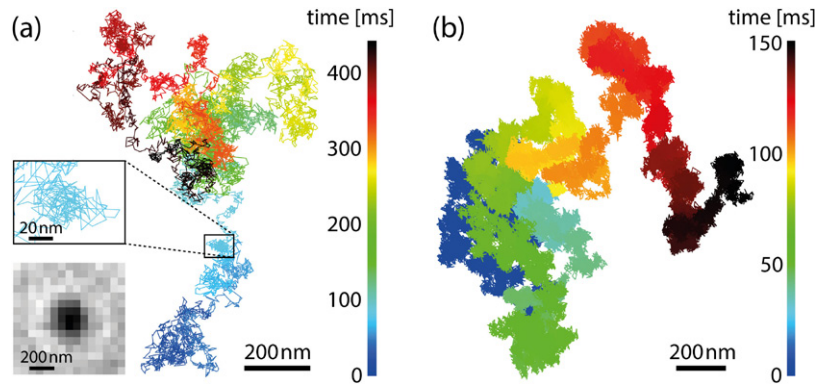


Figure 3. High-speed tracking of lipid diffusion using a GNP as label. (a) Trajectory of a 5 nm GNP bound to a biotinylated DOPE lipid via streptavidin in a DOPC SLB recorded at 23 kHz frame rate for 0.44 s. The illumination intensity at the objective was $0.9 \text{ mW } \mu\text{m}^{-2}$ and the localization precision is 5 nm. The upper inset shows a zoom into a confinement region. The lower inset shows a background-corrected iSCAT image of a 5 nm GNP on a lipid membrane. (b) Trajectory of a 20 nm GNP bound to a biotinylated DOPE lipid in a DOPC SLB recorded at 913 kHz for 0.152 s. The intensity at the objective was $5 \text{ mW } \mu\text{m}^{-2}$.

of working with supported bilayers, we have carried out single lipid diffusion measurements in free-standing membranes of giant unilamellar vesicles (GUVs) [16]. In order to be able to carry out these measurements under physiological conditions, we followed published GUV formation protocols [17, 18] and adjusted them for the growth of GUVs under various salt concentrations [19].

Here, we take advantage of the exquisite 3D tracking capability of iSCAT [20, 21], which relies on the oscillatory change of the propagating phase along the optical axis in the interferometric signal. As an example for 3D tracking, we track Tat₄₇₋₅₇ peptide-coated polymer nanoparticles [22] on a GUV. The Tat₄₇₋₅₇ peptide is derived from HIV-1 Tat protein and is known for its ability to penetrate cells. It is assumed that it exploits the complex cell machinery for uptake [23, 24], but membrane translocation in a passive manner by pore formation had also been reported on model membranes by fluorescence studies [25, 26]. Studying the interaction of such peptides with a pure lipid membrane can help to provide important insight into the functioning.

Figure 4(a) shows an iSCAT image of a Tat-coated polymer particle with a diameter of around 50 nm on a GUV made of DOPC. A large contrast of about 10% enables a localization precision of 2 nm. In addition, we clearly recognize the Newton rings that stem from the interference of the reflections from the GUV and the glass substrate surfaces. Figure 4(b) displays a reconstructed 3D trajectory of a Tat particle diffusing on a DOPC GUV in Tris buffer. The data were recorded at a frame rate of 1 kHz for 10 s. By fitting the cumulative probability of squared step sizes (see [1]), we characterized the diffusion by the peaks of the major and minor mobility distributions at $D_1 = 1.00 \pm 0.01 \text{ } \mu\text{m}^2 \text{ s}^{-1}$ and $D_2 = 4.88 \pm 0.04 \text{ } \mu\text{m}^2 \text{ s}^{-1}$, respectively (figure 4(c)). These two distinct mobilities were observed for almost every trajectory examined. Adding 2 mol-% negatively charged lipids (DOPG) did not change the interaction or the diffusion behaviour of the cationic Tat particles significantly ($D_1 = 1.13 \pm 0.02 \text{ } \mu\text{m}^2 \text{ s}^{-1}$, $D_2 = 5.00 \pm 0.23 \text{ } \mu\text{m}^2 \text{ s}^{-1}$, see figure 4(d)). However, shown in figure 4(e), when adding 150 mM NaCl to the Tris buffer and 30 mol-% DOPE to the lipid solution, an enhanced

interaction could be observed, featured by reduced major and minor mobilities around $D_1 = 0.55 \pm 0.02 \text{ } \mu\text{m}^2 \text{ s}^{-1}$ and $D_2 = 1.91 \pm 0.19 \text{ } \mu\text{m}^2 \text{ s}^{-1}$, respectively. The slower mobility might be caused by aggregation of particles after attaching to the membrane. Indeed, we could directly see aggregation of Tat-coated nanoparticles indicated by the change in the iSCAT contrast (figure 4(f)).

Recently, scientists have reported formation of pores in GUV membranes of 2 nm in size by very small Tat peptides [25]. These efforts investigated the diffusion of single fluorescently labelled Tat peptides on GUV membranes. In our case, we did not identify any translocation of particles through the membrane, which would be detectable via the change in particle contrast. However, we did observe that GUVs started to become leaky after a while and spread on the beta-casein-passivated glass substrate (figure 4(g)); this does not take place in the absence of Tat particles. Further studies are needed to decipher the behaviour of Tat peptides on lipid membranes with nanometer resolution and in real time. Here, we have presented a first report of using iSCAT for 3D tracking of a nanoparticle on a GUV. More extensive studies on tracking gold nanoparticles on curved GUV membranes and the details of 3D tracking are currently in progress and will be published elsewhere.

4. Label-free iSCAT

4.1. Visualizing lipid bilayer formation from single lipid vesicles

As mentioned earlier, the central parameter that determines the sensitivity of iSCAT is the polarizability of the nano-object to be detected. To this end, even individual unlabelled bioparticles can be detected via iSCAT, as exemplified by our earlier reports of the detection of single unlabelled viruses with a diameter of about 45 nm [9, 27]. In this section, we show that iSCAT can also image small lipid vesicles and nanoscopic domains of an SLB.

Figure 5 illustrates a series of images recorded during the process of SLB formation. Following parts (a) to (c), iSCAT reveals the arrival and bursting of individual lipid vesicles to

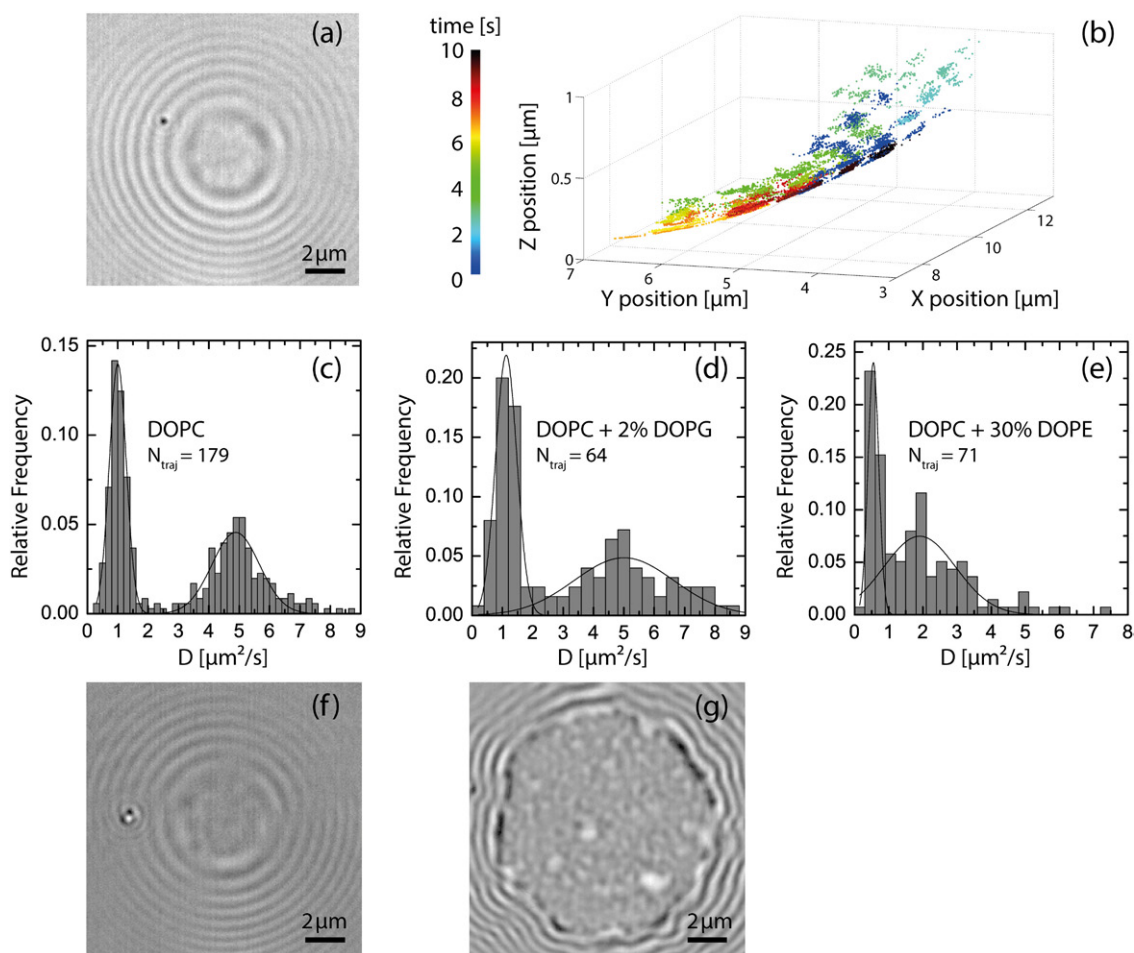


Figure 4. Detection and tracking of Tat-coated polymer particles on GUV membranes in Tris buffer. (a) Background-corrected iSCAT image of a single Tat particle on a DOPC GUV membrane. (b) 3D diffusion trajectory of a Tat particle on a DOPC GUV. (c) Histogram of diffusion coefficients for Tat particles moving on DOPC GUVs. Every trajectory shows two mobilities. From a two-component Gaussian fit (black line) two peaks can be identified at $D_1 = 1.00 \pm 0.01 \mu\text{m}^2 \text{s}^{-1}$ and $D_2 = 4.88 \pm 0.04 \mu\text{m}^2 \text{s}^{-1}$. (d) Histogram of diffusion coefficients for Tat particles moving on DOPC + 2 mol-% DOPG GUVs. Two peaks can be found at $D_1 = 1.13 \pm 0.02 \mu\text{m}^2 \text{s}^{-1}$ and $D_2 = 5.00 \pm 0.23 \mu\text{m}^2 \text{s}^{-1}$. (e) Histogram of diffusion coefficients for Tat particles moving on DOPC + 30 mol-% DOPE GUVs in Tris buffer + 150 mM NaCl. Two peaks can be found at $D_1 = 0.55 \pm 0.02 \mu\text{m}^2 \text{s}^{-1}$ and $D_2 = 1.91 \pm 0.19 \mu\text{m}^2 \text{s}^{-1}$. (f) Background-corrected iSCAT image of a Tat particle cluster on a GUV membrane composed of DOPC + 30 mol-% DOPE in Tris buffer + 150 mM NaCl. (g) GUV membrane spreading on the beta-casein-coated glass substrate around 90 min after adding the Tat-coated particles.

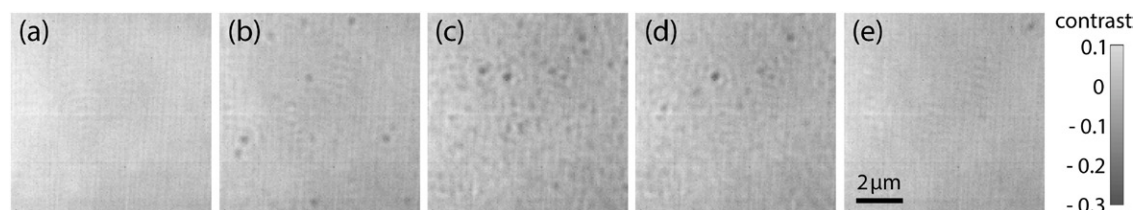


Figure 5. Snap shots showing the formation of a supported lipid membrane. The integration time for each frame was 1 ms. (a) Initial glass surface. The very faint structure is a residual contrast caused by wavefront impurities and glass roughness. This will remain constant throughout. (b) and (c) Arrival of lipid vesicles. The roughness seen in the image is now caused by the contrast (see grey scale) of the lipid vesicles. (d) and (e) Fusion of individual vesicles into a continuous bilayer with a homogeneous refractive index.

produce a lipid membrane, even without the need for background correction or subsequent image processing. The initial smooth glass surface first becomes rougher upon the arrival of small unilamellar vesicles and becomes more homogeneous as the adsorbed vesicles rupture and merge to form a continuous membrane (figures 5(d) and (e)). This process has recently been studied systematically by varying the vesicle size (down to 20 nm) and surface interaction strength [28].

Furthermore, iSCAT has been used to directly image the formation of lipid nanodomains [29], which are supposed to play an important role in cell membranes for trafficking and signalling. Using the excellent temporal and spatial resolution of iSCAT, the diffusion of domains as small as 50 nm as well as domain dynamics including formation, destruction and coalescence could be resolved and characterized in a label-free fashion [29].

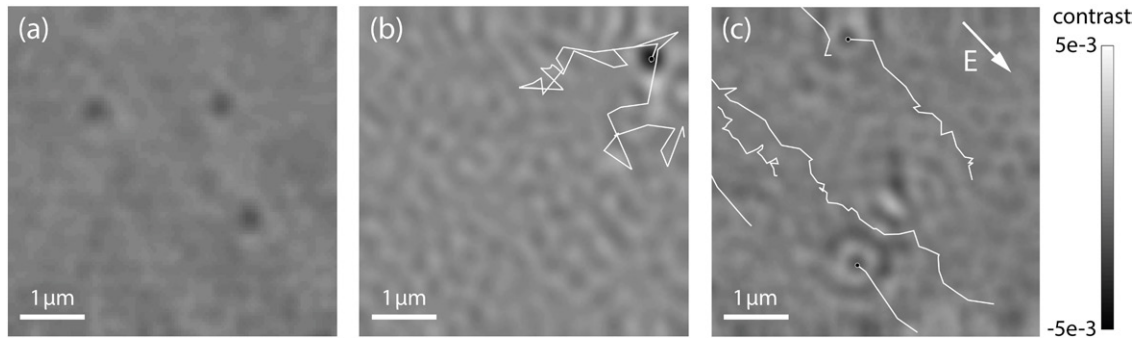


Figure 6. Detection and tracking of unlabelled single proteins. The excitation wavelength was 445 nm and the laser power at the objective was $1 \text{ mW } \mu\text{m}^{-2}$. (a) iSCAT image of three recombinant proteins immobilized on the surface. (b) iSCAT image of a laterally diffusing protein loosely bound to the surface. The thin white line denotes a trajectory of the protein position analyzed from 40 frames. (c) iSCAT snapshot of two proteins and trajectories (40 frames) of the directed motion of proteins in an electric field E with the direction indicated by the white arrow and a field strength of 20 V cm^{-1} . Proteins were denatured and negatively charged using sodium dodecyl sulfate (SDS). The contrast scale corresponds to all subfigures.

4.2. Detecting and tracking single unlabelled proteins

Proteins play a crucial role in almost all processes of life. Methods for the visualization of proteins and their function are, thus, highly in demand. Indeed, various biosensing mechanisms such as surface plasmon resonance sensors have demonstrated the ability to detect sub-monolayers of proteins. In addition, fluorescence labelling allows tracking of single proteins. Recently, we showed that iSCAT can detect single proteins as small as 60 kDa without the need for any labelling [10]. In that work, we imaged the arrival of proteins at a functionalized glass surface and localized their binding sites with 5 nm precision. In addition to recording arrival snapshots, iSCAT has also been elegantly used to investigate the motion of larger proteins such as myosin5 on actin filaments [30].

In figure 6(a), we present an iSCAT image of three *Strep*-tagged recombinant proteins (molecular mass 250 kDa) after landing on a substrate, where the molecules interact non-specifically with the glass surface. Figure 6(b) shows a similar image on a negatively charged surface, where the negatively charged proteins are loosely attracted to the surface by electrostatic interactions bridged by positive ions contained in the buffer. These molecules can move in the lateral plane defined by the substrate. The overlaid trajectory displays diffusion over 10 s (see also video 1 and 2 in supplementary data). In figure 6(c), we applied a lateral electric field and observed directed protein motion. By exploiting the charge-to-mass ratio, it should be possible to combine iSCAT and other analytic methods such as electrophoresis to reach single molecule sensitivity [31]. This capability paves the way for studying the interactions between small biomolecules.

4.3. Looking at a cell membrane

We have seen that iSCAT can detect lipids and proteins without the need for fluorescence labelling as long as the polarizability of the nano-object of interest is large enough, whereby the current detection limit corresponds to a protein mass of the order of tens of kDa. The major challenge in reaching this sensitivity is to distinguish the signal from the background because any sample corrugations or modulations

of the refractive index can provide a large iSCAT signal [8]. In the case of our protein sensing experiment, we addressed this issue by subtracting consecutive images to eliminate the constant signal features and to become sensitive only to the newly arriving proteins. In principle, this approach can be extended to any other situation, where the background is static or changes much more slowly than the phenomenon to be imaged.

A particularly important system to study is the intact membrane of the living cell. Figure 7(a) shows an example of an image of a section of a HeLa cell surface obtained by iSCAT. The strong contrast modulation of the observed speckle pattern poses a serious challenge for recognizing very small particles such as a small protein. However, as figure 7(b) displays, a gold nanoparticle with a diameter of 60 nm or larger can be readily identified. Furthermore, subtraction of the slow movements of the membrane helps to eliminate much of the modulations. Studies of the diffusion of such a particle label will be published elsewhere [32]. We are also currently exploring more advanced imaging and image processing techniques to push the limits of iSCAT for tracking smaller GNPs on cell membranes.

5. Discussion and outlook

In this article, we have provided various examples of studies, where iSCAT can provide new insight in the biophysics of lipids and proteins. In particular, we have emphasized that while these can be tracked at high speed using scattering labels such as gold or polymer nanoparticles, iSCAT can also image unlabelled lipids and proteins as long as the polarizability of the nano-object of interest is large enough. Here, it is important to note that there is no theoretical limit to the size of the particle to be detected, but the limit is a rather practical matter dictated by the nature of the background. In cases, where the background is well characterized, the sensitivity is sufficient to reach single molecule level [10, 33, 34].

An important feature of iSCAT imaging is its ability to reach a large enough signal-to-noise ratio to localize a nanoparticle within a nanometer. In addition, iSCAT can be

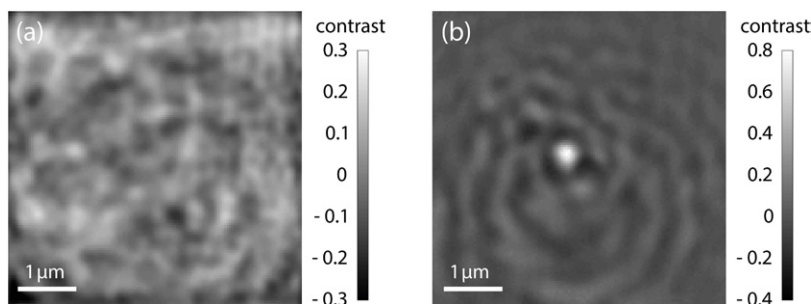


Figure 7. Visualization of a cell membrane using iSCAT. The integration time was $55 \mu\text{s}$ for an illumination intensity of $1 \text{ mW } \mu\text{m}^{-2}$ at the objective. The grey scales show the iSCAT contrast. (a) iSCAT image of the basal membrane of a HeLa cell. The contrast of the membrane corrugations can be as large as 30%. (b) A 60 nm GNP bound to a HeLa cell membrane.

theoretically performed indefinitely fast if a large enough power can be used. Here too, a practical limit is set by the speed and well depth of the available cameras. The size of the particle and the combination of high localization precision and acquisition speed depend on the specific aspects of the system under study.

The measurements discussed in this article find applications in a range of studies, especially on the biophysics of lipid membranes and their interactions with proteins. One of the noteworthy findings concerns the nature of diffusion and domain formation. The data presented in [9] and in figures 2–4 show that a faster and more precise localization procedure reveals nanoscopic features that are not accessible to other methods. These distinctive advantages promise to help understand the remaining open questions.

One difficulty in studying lipid and protein diffusion is to ensure that the GNP attaches to one biomolecule only. Because it is possible that the GNP attaches to its target via multiple linkers and that the linker has several binding sites, it is hard to guarantee that there is only one molecule per particle. In many of our investigations, we try to reach this limit by mixing GNPs with an extremely low concentration of linker molecules so that the latter are under-represented. Another approach is to use very small nanoparticles so that the particle surface area does not leave room for several linkers and bindings. Gold nanoparticles with a diameter of 5 nm get close to this limit.

A further issue is that nanometer localization precision is compromised if the characteristic distance the particle diffuses during one frame is larger than this precision. At an imaging rate of 23 kHz, a lipid with a diffusion coefficient of $1 \mu\text{m}^2 \text{ s}^{-1}$ has a mean step size of 9 nm in one dimension per frame. Thus, much higher localization precisions are smeared due to the lack of speed. The step reduces, on the other hand, to 1 nm if one images at a rate of 1 MHz.

High-speed iSCAT studies require large excitation powers to obtain sufficient number of photons per frame for precise localization. Under these conditions, heating effects have to be considered. For example, an illumination of $5 \text{ mW } \mu\text{m}^{-2}$ is needed for imaging a GNP with a diameter of 20 nm at a localization precision of 9.7 nm within $1 \mu\text{s}$, leading to a temperature increase of about 27 K at its surface [35]. At the same time, measurements using illumination wavelengths and samples, where absorption is negligible, do not suffer from

this restriction. Therefore, depending on the system and its characteristic time and length scales, one has to evaluate the spatiotemporal resolution needed and settle for a tradeoff between the illumination power, label size, temporal resolution and localization precision.

The measurements discussed in this article pave the way for a range of interesting investigations. Lipid vesicles and their fusion with a membrane, intracellular trafficking, endo- and exocytosis, lipid rafts and nanodomain formation, cellular signaling and secretion, and protein–protein interaction are some of the fields where iSCAT can readily contribute to fundamental understanding of biological processes. In addition, iSCAT can be employed in a number of analytical instruments. For example, the exquisite sensitivity and technical simplicity of this method promise to take biosensing to a new performance level. Furthermore, this technique can vastly enhance the detection channel of other analytic tools such as electrophoresis.

Acknowledgments

This work was supported by the Alexander von Humboldt Foundation (fellowship for RWT and professorship for VS), Deutsche Forschungsgemeinschaft (RTG Dynamic Interactions at Biological Membranes and Cluster of Excellence EAM), and the Max Planck Society.

References

- [1] Hsieh C-L, Spindler S, Ehrig J and Sandoghdar V 2014 Tracking single-particles on supported lipid membranes: multimobility diffusion and nanoscopic confinement *J. Phys. Chem. B* **118** 1545–54
- [2] Thompson R E, Larson D R and Webb W W 2002 Precise nanometer localization analysis for individual fluorescent probes *Biophys. J.* **82** 2775
- [3] Ober R J, Ram S and Ward E S 2004 Localization accuracy in single-molecule microscopy *Biophys. J.* **86** 1185
- [4] Clausen M P and Lagerholm B C 2013 Visualization of plasma membrane compartmentalization by high-speed quantum dot tracking *Nano Lett.* **13** 2332–7
- [5] Tero R, Sasaki G, Ujihara T and Urisu T 2011 Anomalous diffusion in supported lipid bilayers induced by oxide surface nanostructures *Langmuir* **27** 9662–5
- [6] Lindfors K, Kalkbrenner T, Stoller P and Sandoghdar V 2004 Detection and spectroscopy of gold nanoparticles using

- supercontinuum white light confocal microscopy *Phys. Rev. Lett.* **93** 037401
- [7] Fujiwara T, Ritchie K, Murakoshi H, Jacobson K and Kusumi A 2002 Phospholipids undergo hop diffusion in compartmentalized cell membrane *J. Cell Biol.* **157** 1071–81
- [8] Ueno H, Nishikawa S, Iino R, Tabata K V, Sakakihara S, Yanagida T and Noji H 2010 Simple dark-field microscopy with nanometer spatial precision and microsecond temporal resolution *Biophys. J.* **98** 2014–23
- [9] Jacobsen V, Stoller P, Brunner C, Vogel V and Sandoghdar V 2006 Interferometric optical detection and tracking of very small gold nanoparticles at a water-glass interface *Opt. Express* **14** 405
- [10] Kukura P, Ewers H, Müller C, Renn A, Helenius A and Sandoghdar V 2009 High-speed nanoscopic tracking of the position and orientation of a single virus *Nat. Methods* **6** 923–7
- [11] Piliarik M and Sandoghdar V 2014 Direct optical sensing of single unlabelled proteins and super-resolution imaging of their binding sites *Nat. Commun.* **5** 4495
- [12] Taylor R W Interference Scattering Microscopy: a guide (in preparation)
- [13] Clausen M P and Lagerholm B C 2011 The probe rules in single particle tracking *Curr. Protein Pept. Sci.* **12** 699–713
- [14] Spillane K M, Ortega-Arroyo J, de Wit G, Eggeling C, Ewers H, Wallace M I and Kukura P 2014 High-speed single-particle tracking of GM1 in model membranes reveals anomalous diffusion due to interleaflet coupling and molecular pinning *Nano Lett.* **13** 5390–7
- [15] Lin Y-H, Chang W-L and Hsieh C-L 2014 Shot-noise limited localization of single 20 nm gold particle with nanometer spatial precision within microseconds *Opt. Express* **22** 9159
- [16] Fenz S F and Sengupta K 2012 Giant vesicles as cell models *Integr. Biol.* **4** 982–95
- [17] Angelova M I and Dimitrov D S 1986 Liposome electroformation *Faraday Discuss. Chem. Soc.* **81** 303–11
- [18] Weinberger A, Tsai F-C, Koenderink G H, Schmidt T F, Itri R, Meier W, Schmatko T, Schröder A and Marques C 2013 Gel-assisted formation of giant unilamellar vesicles *Biophys. J.* **105** 154–64
- [19] Stein H E *et al* in preparation
- [20] Jacobsen V, Klotzsch E and Sandoghdar V 2007 Interferometric detection and tracking of nanoparticles *Nano Biophotonics* vol 3, ed H Masuhara *et al* (Amsterdam: Elsevier)
- [21] Mojarad N, Sandoghdar V and Krishnan M 2013 Measuring three-dimensional interaction potentials using optical interference *Opt. Express* **21** 9377
- [22] Drappier C, Oliveira H, Sandre O, Ibarboure E, Combet S, Garanger E and Lecommandoux S 2013 Self-assembled core-shell micelles from peptide-b-polymer molecular chimeras towards structure-activity relationships *Faraday Discuss.* **166** 83–100
- [23] Ferrari A, Pellegrini V, Arcangeli C, Fittipaldi A, Giacca M and Beltram F 2003 Caveolae-mediated internalization of extracellular HIV-1 Tat fusion proteins visualized in real time *Mol. Ther.* **8** 284–94
- [24] Mishra A *et al* 2011 Translocation of HIV TAT peptide and analogues induced by multiplexed membrane and cytoskeletal interactions *Proc. Natl Acad. Sci.* **108** 16883–8
- [25] Ciobanaru C, Siebrasse J P and Kubitschek U 2010 Cell-penetrating HIV1 TAT peptides can generate pores in model membranes *Biophys. J.* **99** 153–62
- [26] Wheaton S A, Ablan F D O, Spaller B L, Trieu J M and Almeida P F 2013 Translocation of cationic amphipathic peptides across the membranes of pure phospholipid giant vesicles *J. Am. Chem. Soc.* **135** 16517–25
- [27] Ewers H, Jacobsen V, Klotzsch E, Smith A E, Helenius A and Sandoghdar V 2007 Label-free optical detection and tracking of single virions bound to their receptors in supported membrane bilayers *Nano Lett.* **7** 2263–6
- [28] Andrecka J, Spillane K M, Ortega-Arroyo J and Kukura P 2013 Direct observation and control of supported lipid bilayer formation with interferometric scattering microscopy *ACS Nano* **7** 10662–70
- [29] de Wit G, Danial J S H, Kukura P and Wallace M I 2015 Dynamic label-free imaging of lipid nanodomains *Proc. Natl Acad. Sci.* **112** 12299–303
- [30] Ortega Arroyo J, Andrecka J, Spillane K M, Billington N, Takagi Y, Sellers J R and Kukura P 2014 Label-free, all-optical detection, imaging, and tracking of a single protein *Nano Lett.* **14** 2065–70
- [31] Sandoghdar V, Piliarik M and König K *Patent* application pending
- [32] Taylor R W High-speed iSCAT tracking of a single protein on a live cell membrane (in preparation)
- [33] Kukura P, Celebrano M, Renn A and Sandoghdar V 2010 Single-molecule sensitivity in optical absorption at room temperature *J. Phys. Chem. Lett.* **1** 3323–7
- [34] Celebrano M, Kukura P, Renn A and Sandoghdar V 2011 Single-molecule imaging by optical absorption *Nat. Photon.* **5** 95–8
- [35] Gaiduk A, Ruijgrok P V, Yorulmaz M and Orrit M 2010 Detection limits in photothermal microscopy *Chem. Sci.* **1** 343–50